Development of UI-WRF-Chem (v1.0) for the MAIA satellite mission: case demonstration

Huanxin Zhang[1,2], Jun Wang[1,2], Nathan Janechek[1,2], Cui Ge[1,2,‡], Meng Zhou[2,3,§], Lorena Castro García[1,2], Tong Sha[2], Yanyu Wang[2], Weizhi Deng[1,2], Zhixin Xue[1,2], Chengzhe Li[1,2], Lakhima Chutia[1,2], Yi Wang[2], Sebastian Val[4], James L. McDuffie[4], Sina Hasheminassab[4], Scott E. Gluck[4], David J. Diner[4], Peter R. Colarco[5], Arlindo M. da Silva[6]

[1]Department of Chemical and Biochemical Engineering, The University of Iowa, Iowa City, IA, 52242, United States
[2]Center for Global and Regional Environmental Research, The University of Iowa, Iowa City, IA, 52242, United States
[3]Interdisciplinary Graduate Program in Geo-Informatics, The University of Iowa, Iowa City, IA, 52242, United States
[4]NASA Jet Propulsion Laboratory, California Institute of Technology, Pasadena, CA, 91109, United States
[5]Atmospheric Chemistry and Dynamics Lab, NASA Goddard Space Flight Center, Greenbelt, MD, 20771, United States
[6]Global Modeling and Assimilation Office, NASA Goddard Space Flight Center, Greenbelt, MD, 20771, United States

[‡]Currently at: South Coast Air Quality Management District (AQMD), Diamond Bar, CA, 91765, United States
[§]Currently at: Goddard Earth Sciences Technology and Research (GESTAR) II, University of Maryland, Baltimore County, Baltimore, MD, 21250, United States

Correspondence to: Huanxin Zhang (huanxin-zhang@uiowa.edu), Jun Wang (jun-wang-1@uiowa.edu)

Text S1. Ground and satellite observation datasets

Surface observation of meteorological variables including air temperature at 2m (t2), dew temperature at 2m (dewt2), wind speed at 10m (wspd10) and sea level pressure (pres) used in CHN-Beijing are obtained from the Meteorological Information Comprehensive Analysis and Process System (MICAPS) in China. Surface observations of meteorological variables of t2, dewt2, wspd10 and pres used for ITA-Rome and USA-Atlanta evaluation are from the Integrated Surface Database (ISD). Surface observations of meteorological variables of t2, relative humidity (RH), wspd10 and pres used for USA-LosAngeles evaluation are downloaded from the pre-generated data files via the U.S. Environmental Agency (EPA)'s website (https://aqs.epa.gov/aqsweb/airdata/download_files.html#Raw). Surface observations of hourly $PM_{2.5}$ and PM_{10} mass concentration used in CHN-Beijing are from environmental monitoring stations managed by the Ministry of Environmental Protection in China. Surface observation of hourly $PM_{2.5}$ and PM_{10} concentration used in USA-LosAngeles and USA-Atlanta are also from the U.S. EPA's website. Surface observations of daily $PM_{2.5}$ and PM_{10} concentration used in ITA-Rome are from the MAIA Surface Monitor Data Product downloaded from Earthdata Search.

The ground-based Aerosol Robotic Network (AERONET) provides global observations of AOD, which is available at some or all of the spectral band centered at 340, 380, 440, 500, 670, 940, and 1020 nm (Holben et al., 1998). To compare with UI-WRF-Chem simulated AOD here, AERONET AOD at 440 and 670 nm are interpolated to 550 nm using the Angstrom Exponent provided by the AERONET site. In the current work, we use Version 3 Level 2.0 AOD for CHN-Beijing and USA-LosAngeles and

Level 1.5 AOD for ITA-Rome (Fig 1), which are both cloud-screened. The AERONET inversion algorithm also provides column-integrated aerosol volume size distribution (AVSD) data. The size distribution is binned at 22 logarithmically equidistant discrete points within the radius ranging from 0.05 to 15 μm (Dubovik and King, 2000). Here, we use Version 3 Level 1.5 AVSD data to compare with MERRA-2 calculated AVSD. In addition, the AERONET includes the aerosol spectral deconvolution algorithm (SDA) that infers the fine- and coarse-mode AOD at 500 nm. We use the fine mode fraction (FMF) of AOD at 500 nm here from Version 3 Level 1.5 SDA products to identify dust events.

The Moderate Resolution Imaging Spectrometer (MODIS) instrument on board Terra and Aqua has a swath of ~2,330 km, allowing a global coverage every 1 or 2 days. Terra and Aqua cross the equator at about ~10:30 am LT and ~1:30 pm LT, respectively. Here, we use the MODIS level 2 Collection 6.1 (C6.1) Deep Blue (DB) (Hsu et al., 2019) AOD products at 550 nm from Aqua, denoted as MYD04. We also use MODIS land products including the Land Cover product and the Land Surface Temperature (LST) product. The MODIS Land Cover product (MCD12Q1) (Friedl et al., 2002) with a spatial resolution of 500 m at annual time step is used here. This product includes five different land cover classification schemes, and we have chosen the International Geosphere-Biosphere Program (IGBP) scheme, which identifies 17 land types. We use the MODIS Version 6.1 LST product from Terra (MOD11A) and Aqua (MYD11A) with a spatial resolution of 1 km, which is retrieved using the split-window algorithm. The products provide the LST two times a day, one at daytime (~10:30 am and 1:30 pm LT) and one at nighttime (~22:30 pm and 1:30 am LT). The Visible Infrared Imaging Radiometer Suite (VIIRS) sensor onboard the Suomi-NPP satellite has a swath of ~3,000 km, enabling a global coverage every day. The Suomi-NPP satellite crosses the equator at about ~1:30 pm LT. Here, we use the VIIRS Level 2 Version 2.0 (V2.0) DB AOD products at 550 nm.

The Cloud-Aerosol Lidar with Orthogonal Polarization (CALIOP) onboard the Cloud-Aerosol Lidar and Infrared Pathfinder Satellite Observation (CALIPSO) satellite, launched in April 2006, provides vertical distribution information of both aerosols and clouds (Winker et al., 2009). CALIOP Level 2 processing algorithm first separates aerosol and cloud layers, then determines the aerosol type (clean marine, mineral dust, polluted continental/smoke, clean continental, polluted dust, elevated smoke, and dusty marine), and finally retrieves the particle backscatter and extinction coefficient. Here, we use the Level 2 aerosol products with a horizonal resolution of 5 km and a vertical resolution of 30 m below 8.2 km, 60 m for 8.2–20.2 km, and 180 m for 20.2–30.1 km. The TROPOspheric Monitoring Instrument (TROPOMI) instrument, onboard the European Space Agency (ESA) Sentinel-5 Precursor (S-5P) satellite, launched in October 2017. It has a nearly global daily coverage with an overpass time of ~1:30 pm LT. Here, we use the TROPOMI Level 2 NO_2 column densities with a horizontal spatial resolution of 3.5 x 7 km^2. We exclude pixels that has cloud fraction over 30% and Quality Assurance (QA) values less than 0.5. When comparing model NO_2 columns with TROPOMI data, the averaging kernels (AK) provided in the TROPOMI NO_2 product are used. The Global Precipitation Measurement (GPM) mission (Hou et al., 2014), launched the GPM Core Observatory satellite in February, 2014 and has since provided precipitation data on a global scale. The Integrated Multi-satellitE Retrievals for GPM (IMERG) algorithm is used for intercalibrating, merging and interpolating multiple satellite

precipitation estimates as well as precipitation gauge analyses. Here, we use the IMERG Version 07 (V07) final run precipitation product with a spatial resolution of 0.1° x 0.1° and temporal resolution of 30 minutes.

Text S2. Selection of physics schemes used in UI-WRF-Chem for target areas

For each target area, we focus on the selection of the following physics scheme: microphysics, longwave radiation, shortwave radiation, and planetary boundary layer (PBL). For each target area, we first conduct literature review to find the commonly used schemes. Then, we conduct our own sensitivity tests to select the optimal combination of the schemes. Since CHN-Beijing has relative higher aerosol loading, we run WRF-Chem to carry out the sensitivity runs but for other target areas, we have only conducted WRF only runs to save the computational cost. Table S1 shows the suite of sensitivity simulation conducted over CHN-Beijing, ITA-Rome, USA-LosAngeles, and USA-Atlanta for July 2018, June 2023, July 2018 and June 2022 respectively. Figure S1 and Table S2 show the statistics for evaluating model simulated hourly or 3-hourly meteorology variables including air temperature t2, dewt2 or RH, wspd10 and pres. We find that no single sensitivity simulation can result in the best performance for all the meteorology variables evaluated, which is also found in the literature (e.g. (Chen et al., 2017)). We select simulation 1, simulation 2, simulation 1, simulation 1 as the final configuration for CHN-Beijing, ITA-Rome, USA-LosAngeles and USA-Atlanta, respectively.

Table S1. A suite of UI-WRF-Chem sensitivity simulations with different options of physics schemes over CHN-Beijing, ITA-Rome, USA-LosAngeles and USA-Atlanta target areas.

Target area	Simulation number	Microphysics	Longwave	Shortwave	PBL
Beijing	1	Lin	RRTMG	RRTMG	YSU
	2	Morrison	RRTMG	RRTMG	YSU
	3	Lin	RRTMG	RRTMG	MYJ
	4	Lin	RRTM	Goddard	YSU
Rome	1	Lin	RRTMG	RRTMG	YSU
	2	Morrison	RRTMG	RRTMG	YSU
	3	WSM6	RRTMG	RRTMG	YSU
	4	Morrison	RRTMG	RRTMG	MYJ
	5	Morrison	RRTMG	RRTMG	MYNN2.5
	6	Morrison	RRTM	Goddard	YSU
Los Angeles	1	Li	RRTMG	RRTMG	YSU
	2	Lin	RRTMG	RRTMG	MYJ
	3	Lin	RRTM	Goddard	YSU
Atlanta	1	Lin	RRTMG	RRTMG	YSU
	2	Morrison	RRTMG	RRTMG	YSU
	3	WSM6	RRTMG	RRTMG	YSU
	4	Lin	RRTMG	RRTMG	MYJ
	5	Lin	RRTMG	RRTMG	MYNN2.5
	6	Lin	RRTM	Goddard	YSU

Table S2. Statistics for comparing UI-WRF-Chem simulated meteorological variables with ground observations for CHN-Beijing, ITA-Rome, USA-LosAngeles and USA-Atlanta target areas.

Target area	Simualtion number	t2			dewt2/RH			wspd10			pres		
		MB	RMSE	R	MB	RMSE	R	MB	RMSE	R	MB	RMSE	R
Beijing	1	1.02	2.26	0.85	-1.13	1.97	0.76	0.89	1.75	0.44	-0.55	1.07	0.96
	2	1.33	2.54	0.83	-0.78	1.97	0.69	1.07	1.92	0.44	-0.94	1.40	0.95
	3	0.96	2.36	0.84	-0.87	1.77	0.78	1.87	2.60	0.41	-0.54	1.10	0.95
	4	1.21	2.47	0.84	-1.11	2.08	0.72	1.06	1.91	0.43	-0.87	1.33	0.95
Rome	1	0.63	2.30	0.87	-0.60	2.99	0.59	-0.09	1.80	0.48	-0.38	1.21	0.89
	2	0.63	2.27	0.87	-0.61	2.93	0.61	-0.14	1.78	0.48	-0.34	1.17	0.90
	3	0.67	2.31	0.87	-0.56	2.97	0.59	-0.08	1.80	0.48	-0.37	1.19	0.90
	4	0.72	2.23	0.88	-0.28	2.99	0.59	1.04	2.26	0.50	-0.27	1.09	0.91
	5	0.29	2.21	0.87	-0.77	2.95	0.61	0.41	1.84	0.52	-0.18	1.09	0.90
	6	1.01	2.50	0.86	-0.28	2.98	0.58	0.15	1.98	0.43	-1.18	1.99	0.81
LA	1	0.94	3.09	0.91	-6.47	14.56	0.84	0.29	1.78	0.45	-6.66	9.96	0.99
	2	1.69	3.49	0.90	-8.30	15.39	0.82	1.85	2.90	0.51	-6.66	9.96	0.99
	3	0.98	3.10	0.91	-6.0	14.70	0.83	1.14	2.24	0.50	-6.64	9.96	0.99
Atlanta	1	1.46	2.89	0.86	-1.32	3.02	0.77	0.67	1.86	0.23	-0.27	2.51	0.82
	2	1.52	2.87	0.87	-1.41	3.08	0.76	0.64	1.82	0.23	-0.18	2.50	0.82
	3	1.49	2.90	0.87	-1.24	2.97	0.77	0.69	1.88	0.23	-0.28	2.51	0.82
	4	1.24	2.83	0.87	-0.83	2.70	0.77	2.17	3.03	0.31	-0.21	2.50	0.82
	5	1.03	2.67	0.88	-1.50	3.08	0.77	1.64	2.53	0.32	-0.17	2.50	0.82
	6	1.71	3.07	0.86	-1.30	3.02	0.77	0.76	1.93	0.22	-0.55	2.59	0.81

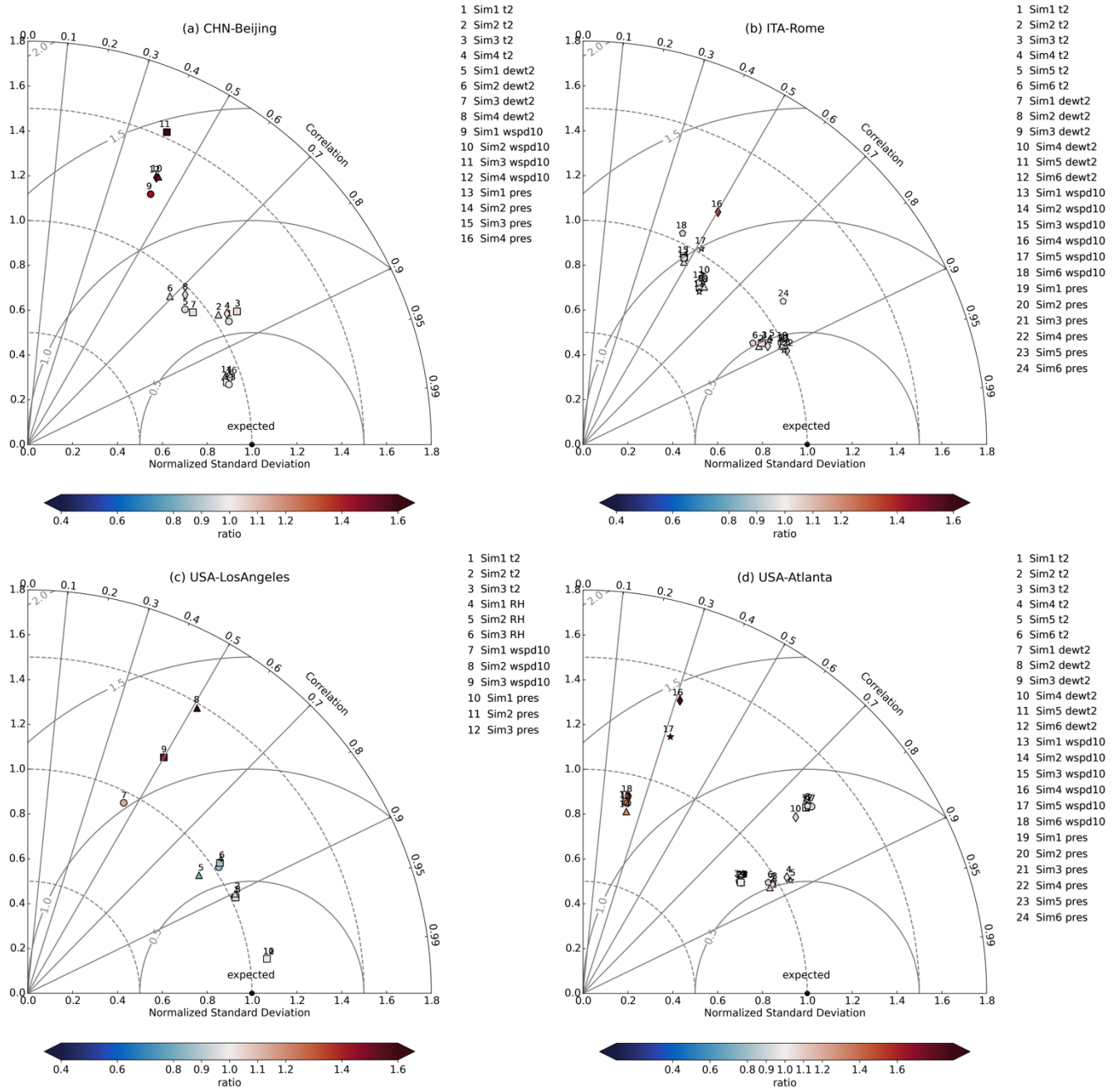

Figure S1. Taylor diagrams for evaluating UI-WRF-Chem model simulated meteorological variables (t2, dewt2 or RH, wspd10 and pres) with ground observations for: (a) CHN-Beijing, (b) ITA-Rome, (c) USA-LosAngeles and (d) USA-Atlanta. Sim1-Sim6 corresponds to the sensitivity simulations 1–6 in Table S1, which are represented by the circle, triangle, square, diamond, star and pentagon, respectively. Color bars represent the ratio between model results and ground observations.

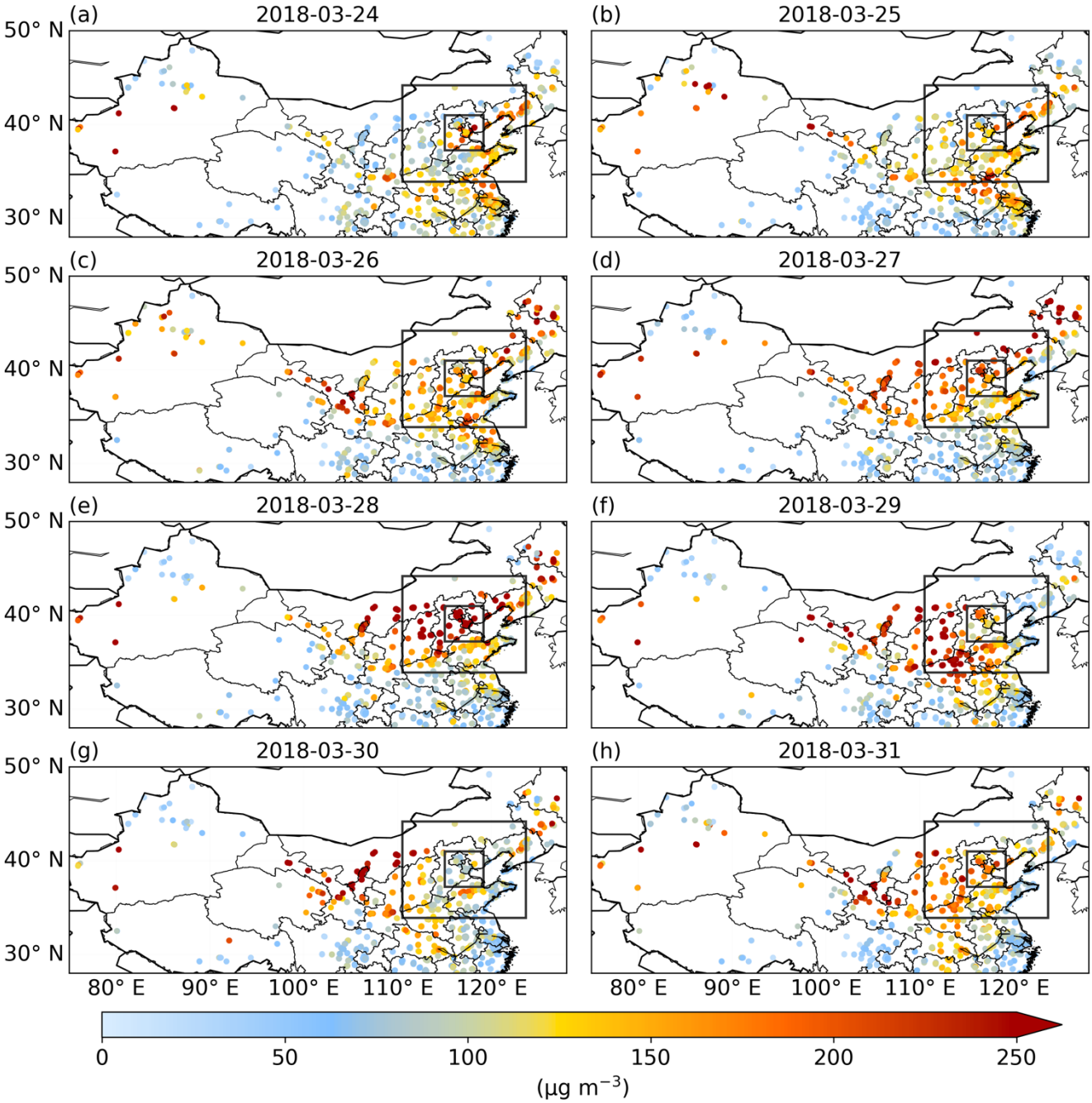

Figure S2. (a)–(h) Observations of daily surface PM_{10} concentration over China from 24–31 March 2018. The gray boxes represent the UI-WRF-Chem 2 nested domains for CHN-Beijing.

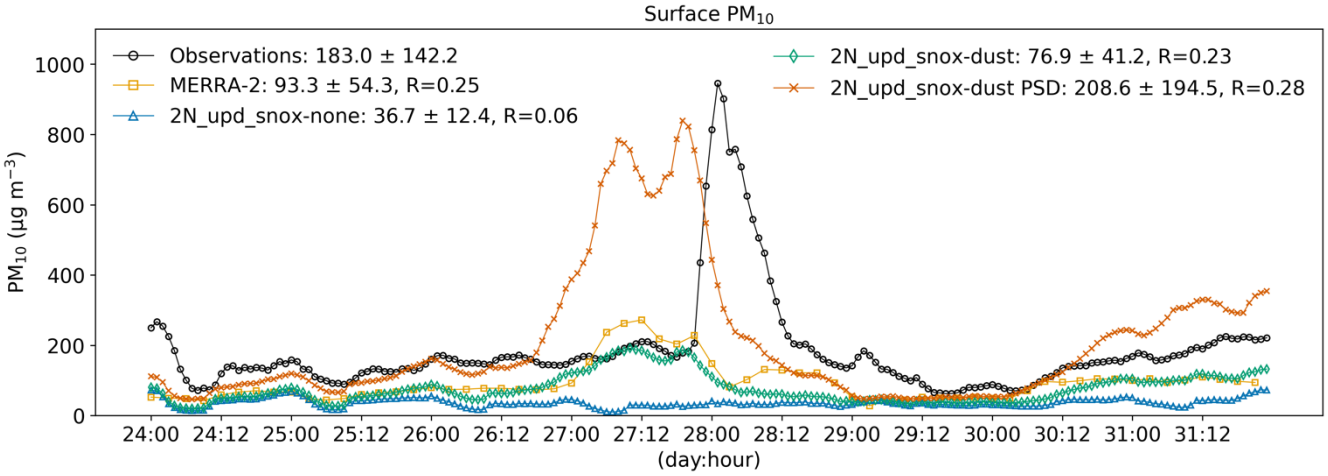

Figure S3. Time series of hourly surface PM_{10} concentration averaged over surface sites in the inner domain (D2) of CHN-Beijing, for 24–31 March 2018, from model simulations and ground observations. 2N_upd_snox-none/dust/dust PSD refer to the UI-WRF-Chem sensitivity simulations with different chemical boundary conditions being considered using MERRA-2 data (Table 1): no chemical species; dust and other aerosols; dust concentration is scaled based on constraining MERRA-2 dust PSD data with AERONET PSD climatology data. Also shown on the plot the is the mean ± standard deviation of surface PM_{10} for model simulations and observations as well as the correlation coefficient (R).

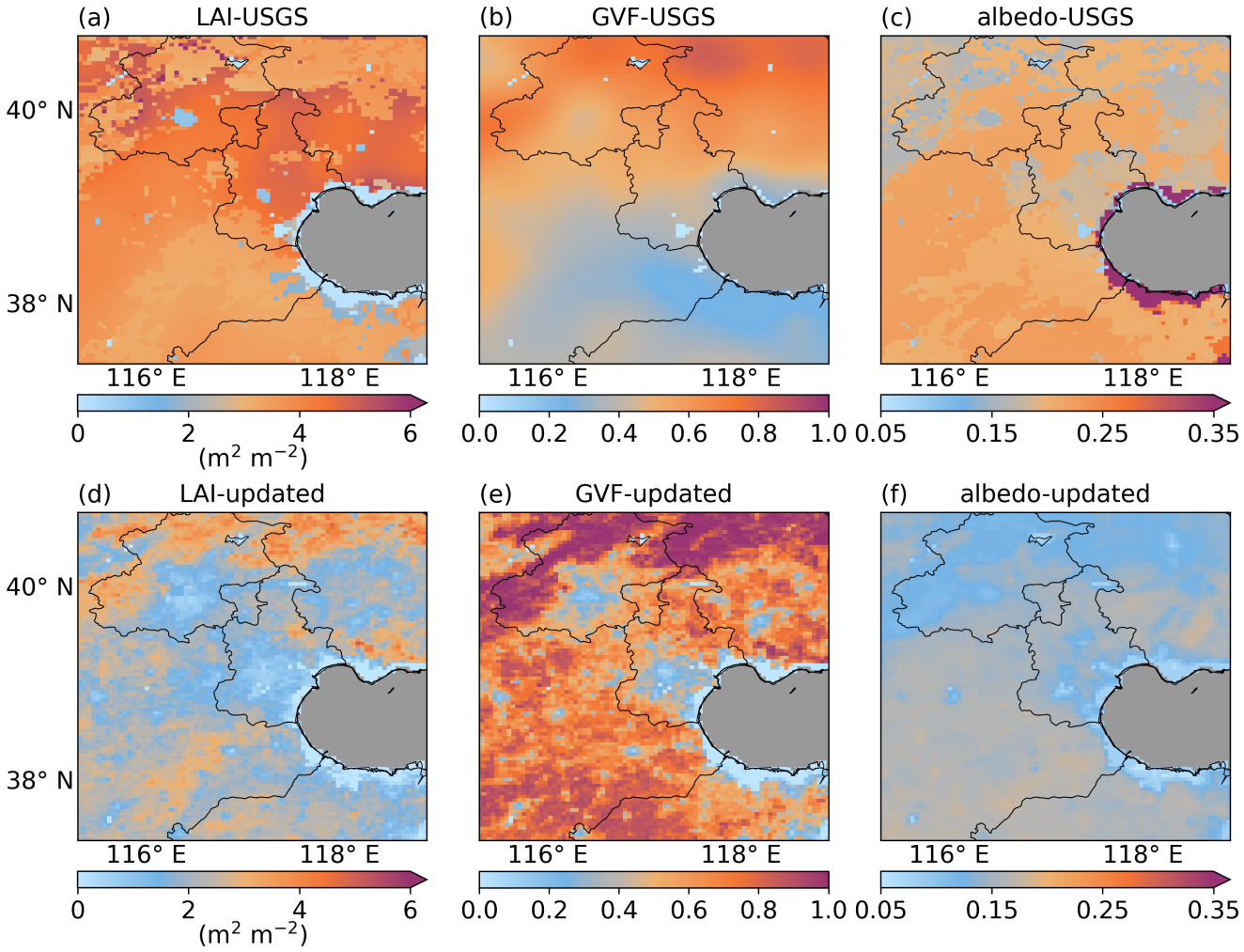

130 Figure S4. Land surface properties used in UI-WRF-Chem sensitivity simulations over CHN-Beijing for July 2018. (a) leaf area index (LAI), (b) green vegetation fraction (GVF), and (c) albedo. (a)–(c) are derived based on the USGS land cover type data. (d)–(f) are the same as (a)–(c) but updated with the 2018 MODIS land data. Oceans are masked as grey colors on the plots.

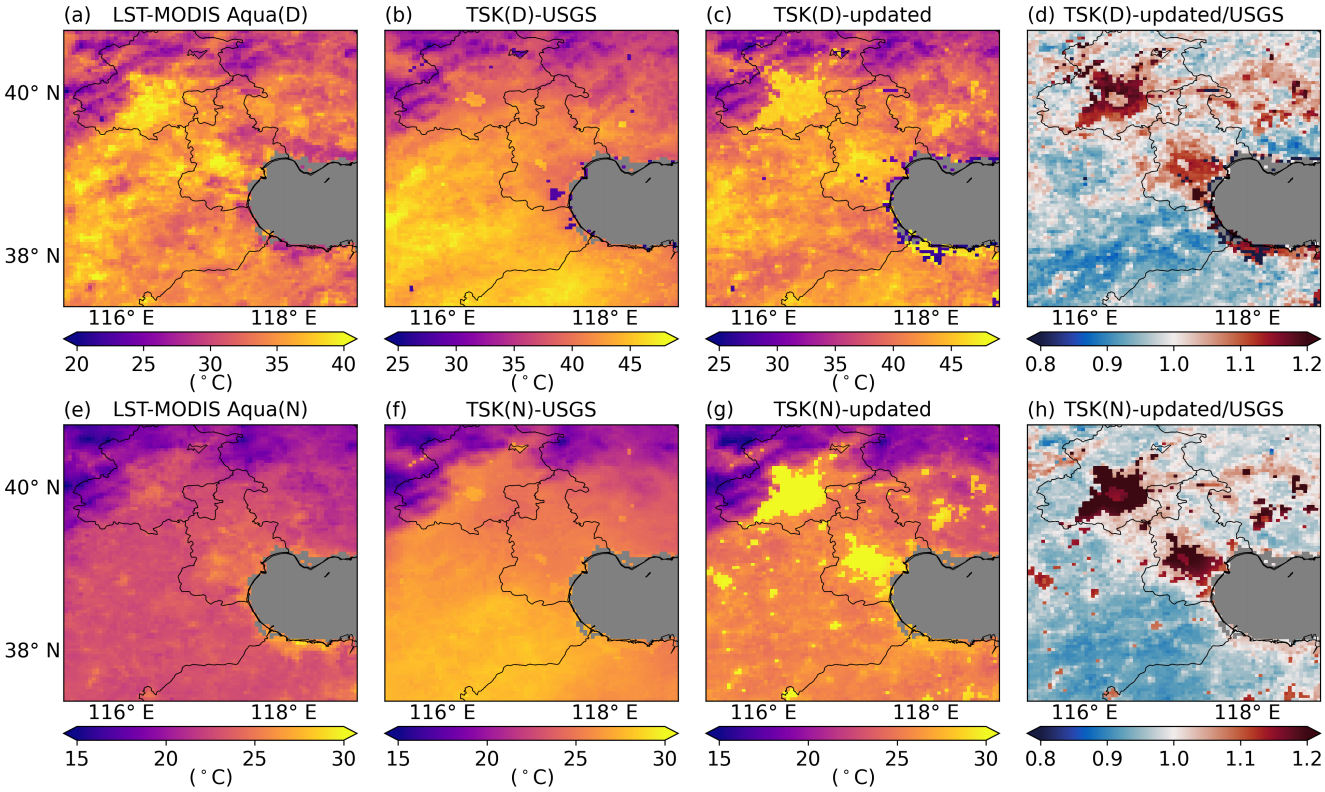

Figure S5. Comparison of UI-WRF-Chem simulated surface skin temperature (TSK) with MODIS Aqua observed land surface temperature (LST) for CHN-Beijing in July 2018. (a) and (e) are the MODIS Aqua LST during daytime (D) and nighttime (N), respectively. (b) and (c) are model simulated TSK averaged over Aqua overpass time during daytime from UI-WRF-Chem sensitivity simulations 2N_def (default USGS land cover type and subsequently derived GVF, LAI and albedo) and 2N_upd (updated land cover type, GVF, LAI and albedo with 2018 MODIS land data) in Table 1, respectively. (d) is the ratio between (c) and (b). (f)–(h) are the same as (b)–(d) but averaged over Aqua overpass time during nighttime. Oceans are masked as grey colors on the plots.

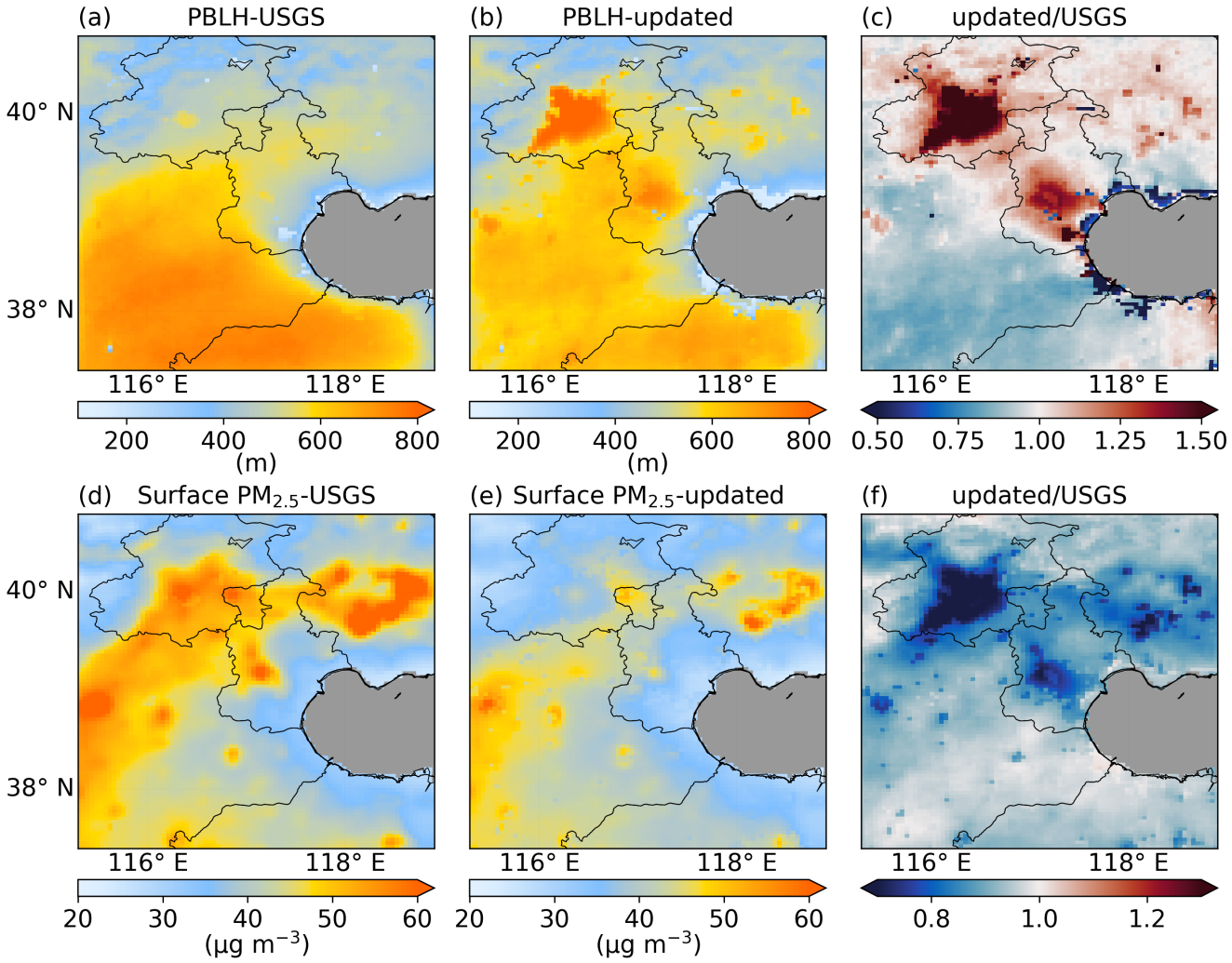

Figure S6. UI-WRF-Chem simulated monthly mean PBLH and surface $PM_{2.5}$ concentration over CHN-Beijing for July 2018. (a) and (b) are model simulated PBLH from the UI-WRF-Chem sensitivity simulation 2N_def (default USGS land cover type and subsequently derived GVF, LAI and albedo) and 2N_upd (updated land cover type, GVF, LAI, and albedo with 2018 MODIS land data) in Table 1 respectively. (c) is the ratio of (b) and (a). (d)–(f) are the same as (a)–(c) but for surface $PM_{2.5}$ concentration. Oceans are masked as grey colors on the plots.

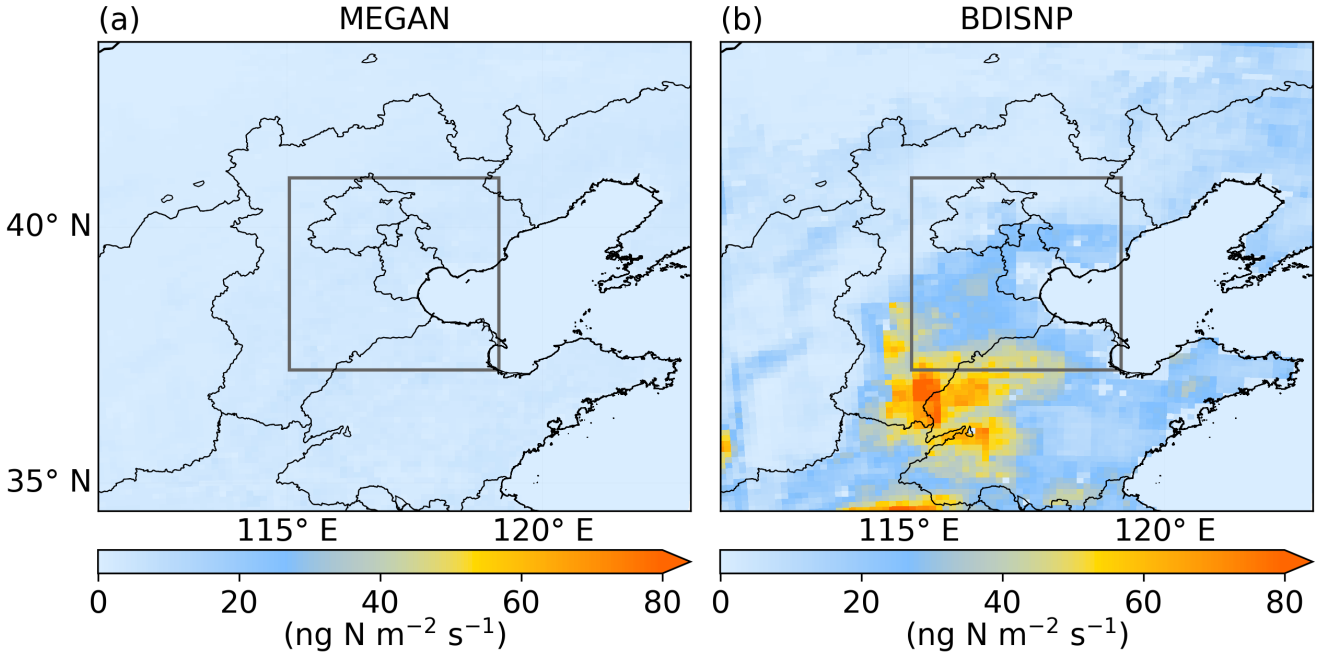

Figure S7. UI-WRF-Chem simulated monthly mean soil NO_x emissions over the outer domain (D1) of CHN-Beijing for July 2018 from different sensitivity simulations in Table 1: (a) using the MEGAN scheme to calculate soil NO_x emissions (2N_upd_MEGAN); (b) using the updated BDISNP scheme to calculate soil NO_x emissions (2N_upd_BDISNP). The gray box represents the inner domain (D2).

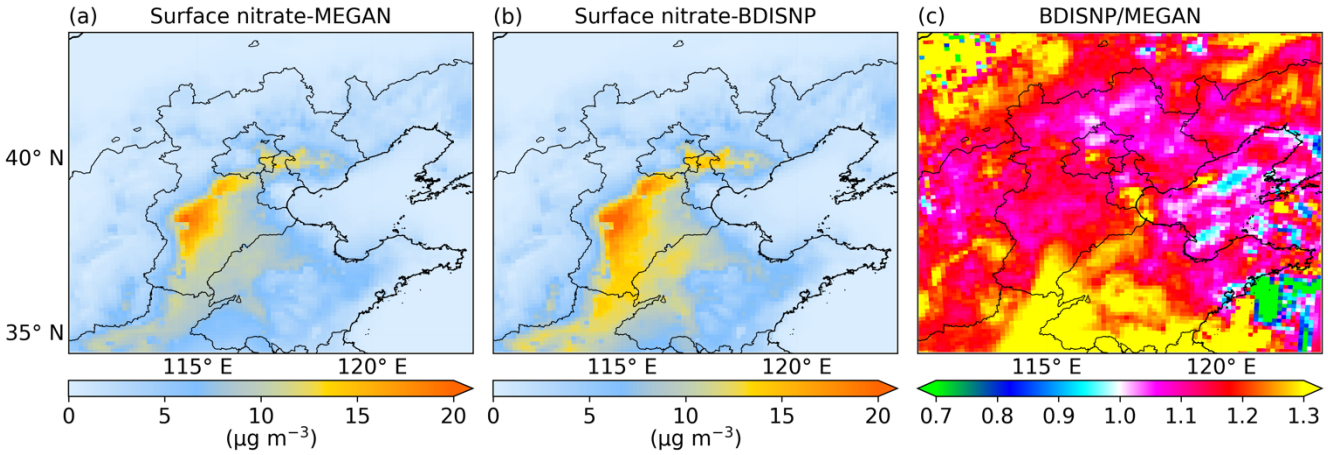

Figure S8. UI-WRF-Chem simulated monthly mean surface nitrate over the outer domain (D1) of CHN-Beijing for July 2018, from different sensitivity simulations in Table 1: (a) using the MEGAN scheme to calculate soil NO_x emissions (2N_upd_MEGAN); (b) using the updated BDISNP scheme to calculate soil NO_x emissions (2N_upd_BDISNP). (c) is the ratio between (b) and (a).

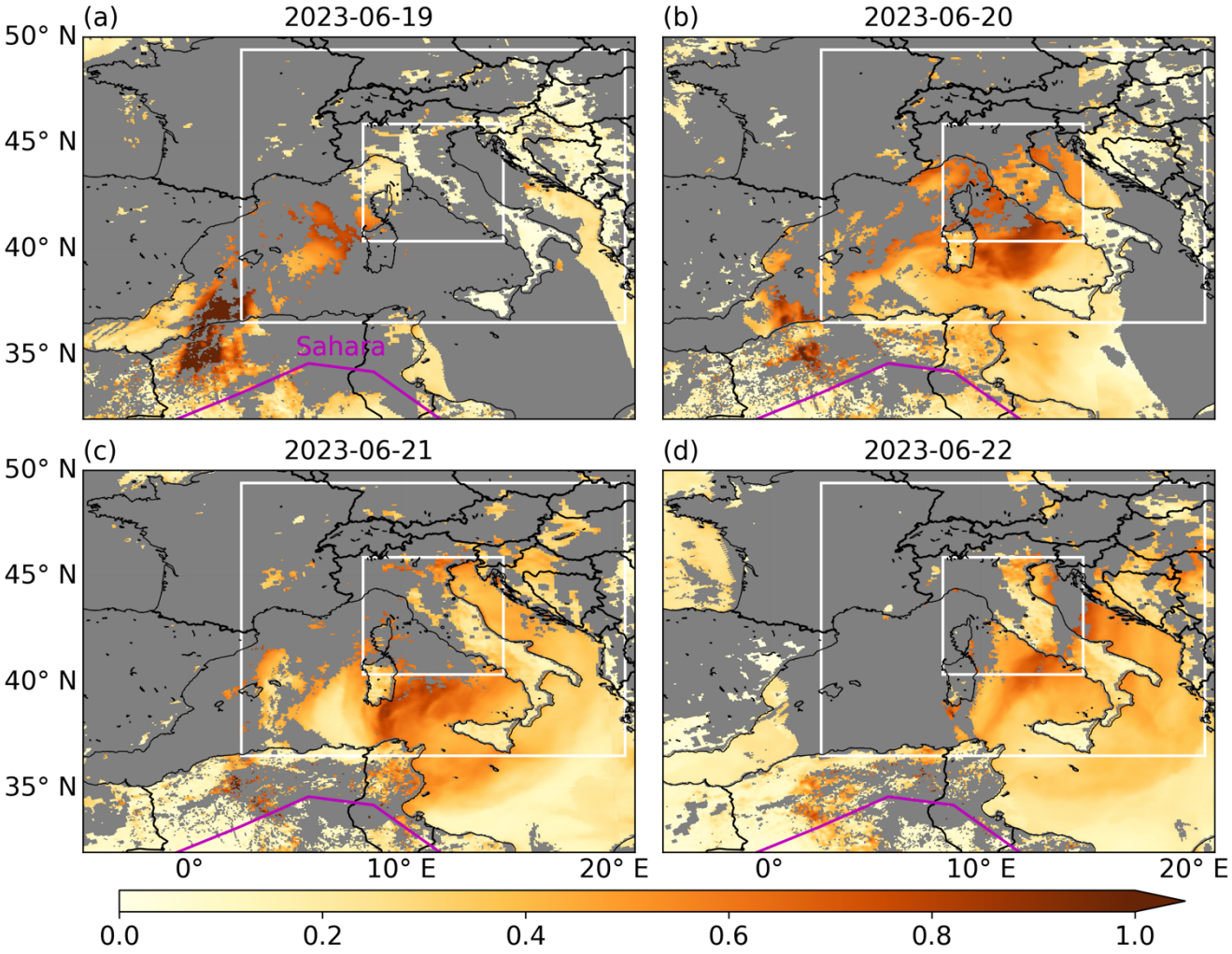

Figure S9. (a)–(d) VIIRS Deep Blue (DB) AOD from 19–22 June 2023. The white boxes represent the UI-WRF-Chem 2 nested domains for outer (D1) and inner domain (D2) of ITA-Rome target area, respectively. The magenta lines represent the boundary of Sahara Desert.

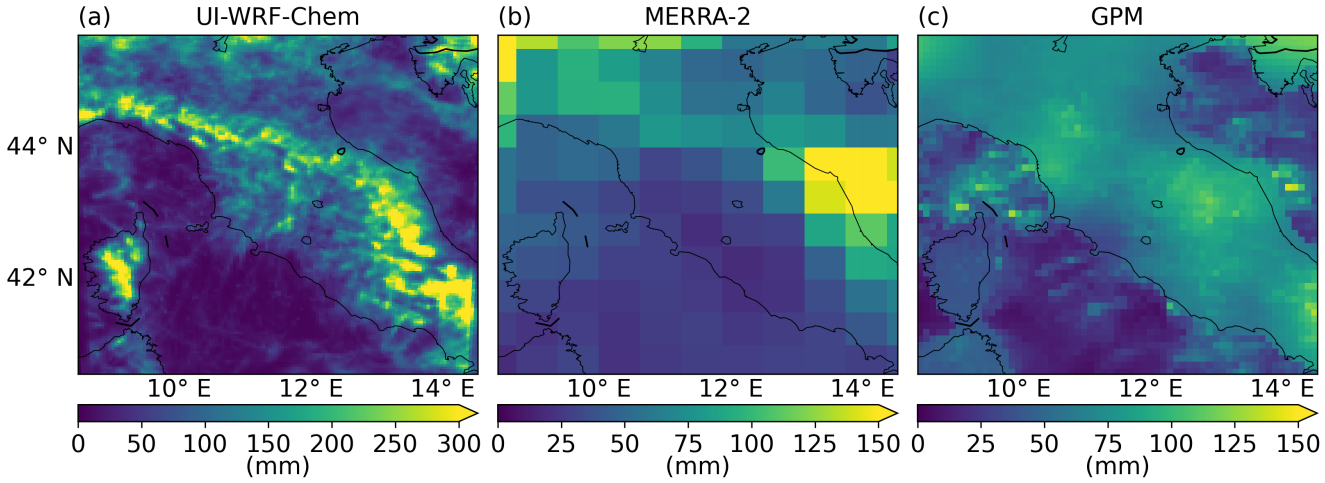

Figure S10. Total precipitation in June 2023 over inner domain (D2) of ITA-Rome from (a) UI-WRF-Chem model simulation, (b) MERRA-2 and (c) GPM IMERG final run precipitation products.

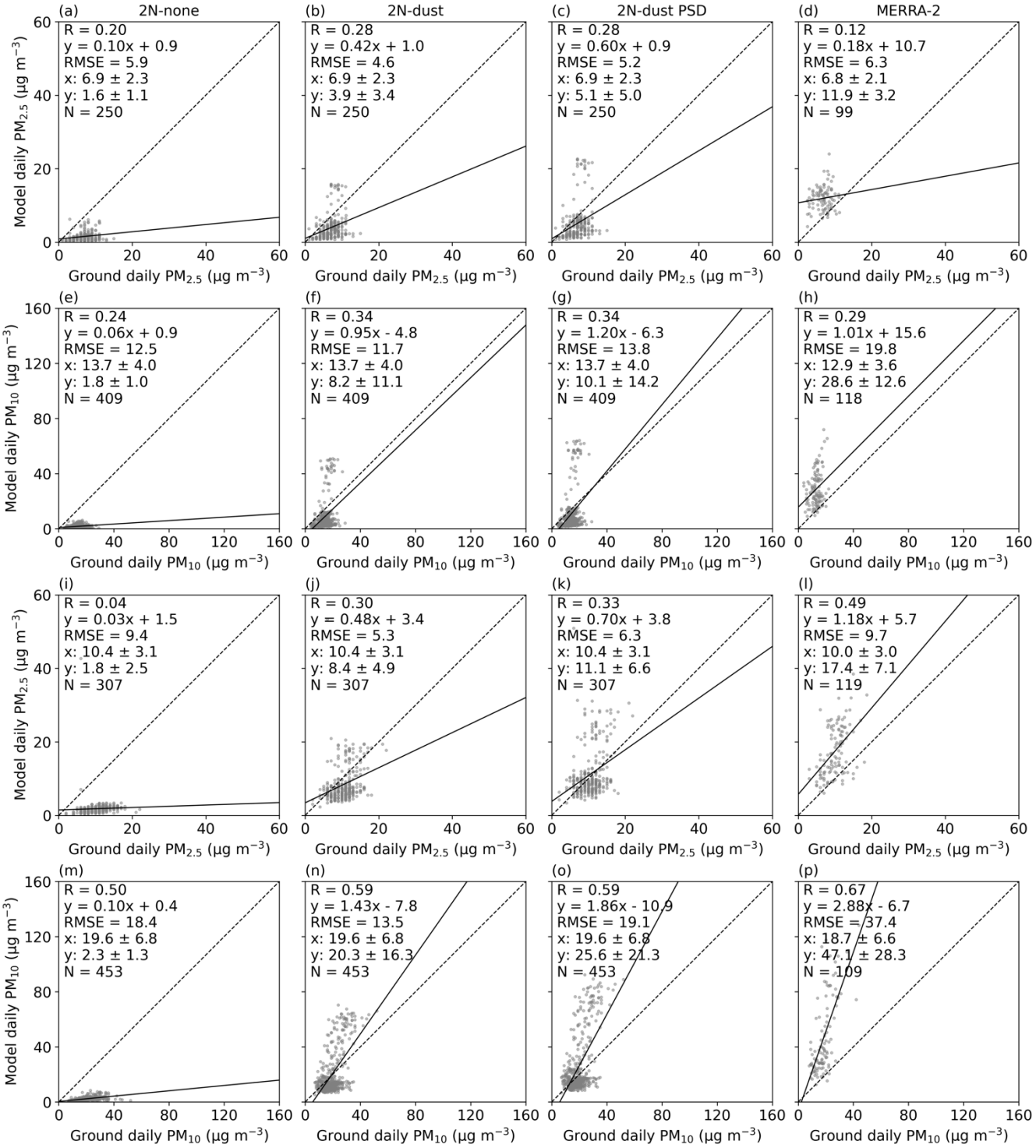

Figure S11. Scatter plot of daily $PM_{2.5}$ ((a)–(d), (i)–(l)) and PM_{10} ((e)–(h), (m)–(p)) between model (y axis) and ground observation (x axis) over the inner domain (D2) of ITA-Rome for June 2023. (a)–(h) are for the first half of June and (i)–(p), are for the second half of

June. (a)–(c), (e)–(g), (i)–(k), and (m)–(o) represent the UI-WRF-Chem sensitivity simulations with different chemical boundary conditions being considered using MERRA-2 data. 2N-none: no chemical species; 2N-dust: dust and other aerosols; 2N-dust PSD: same as 2N-dust except that the dust concentration is scaled based on constraining MERRA-2 dust PSD data with AERONET PSD climatology data. Also shown on the scatter plot is the correlation coefficient (R), the root-mean-square error (RMSE), the mean ± standard deviation for observed (x) and model-simulated surface $PM_{2.5}/PM_{10}$ (y), the number of collocated data points (N), the best fit linear regression (the solid black line) and the 1:1 line (the dashed black line).

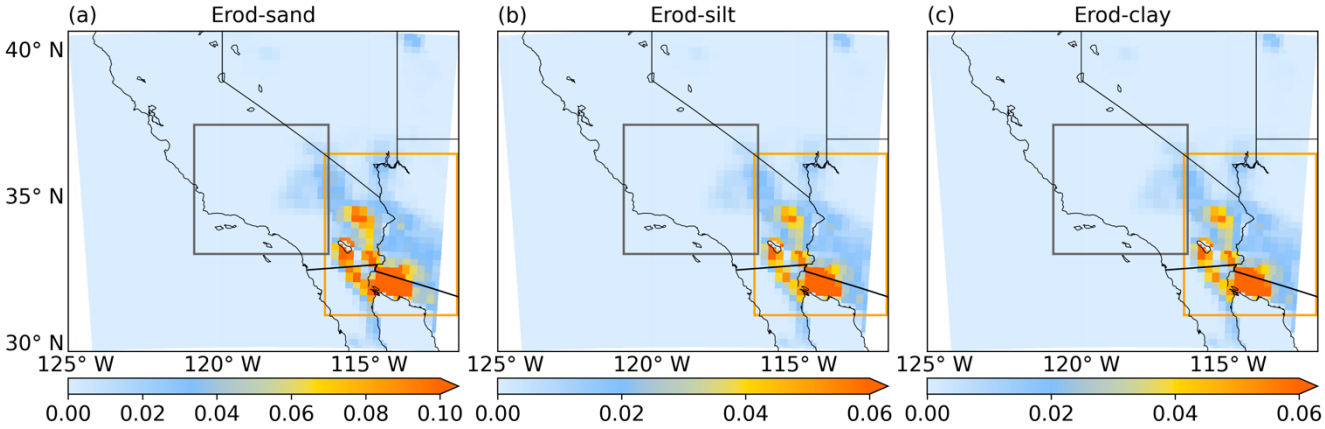

Figure S12. Soil erodibility in UI-WRF-Chem over the outer domain (D1) of USA-LosAngeles for (a) sand, (b) slit and (c) clay. The gray box represents the inner domain (D2). The orange box is defined as the dust-prone region here and used for tuning dust emissions.

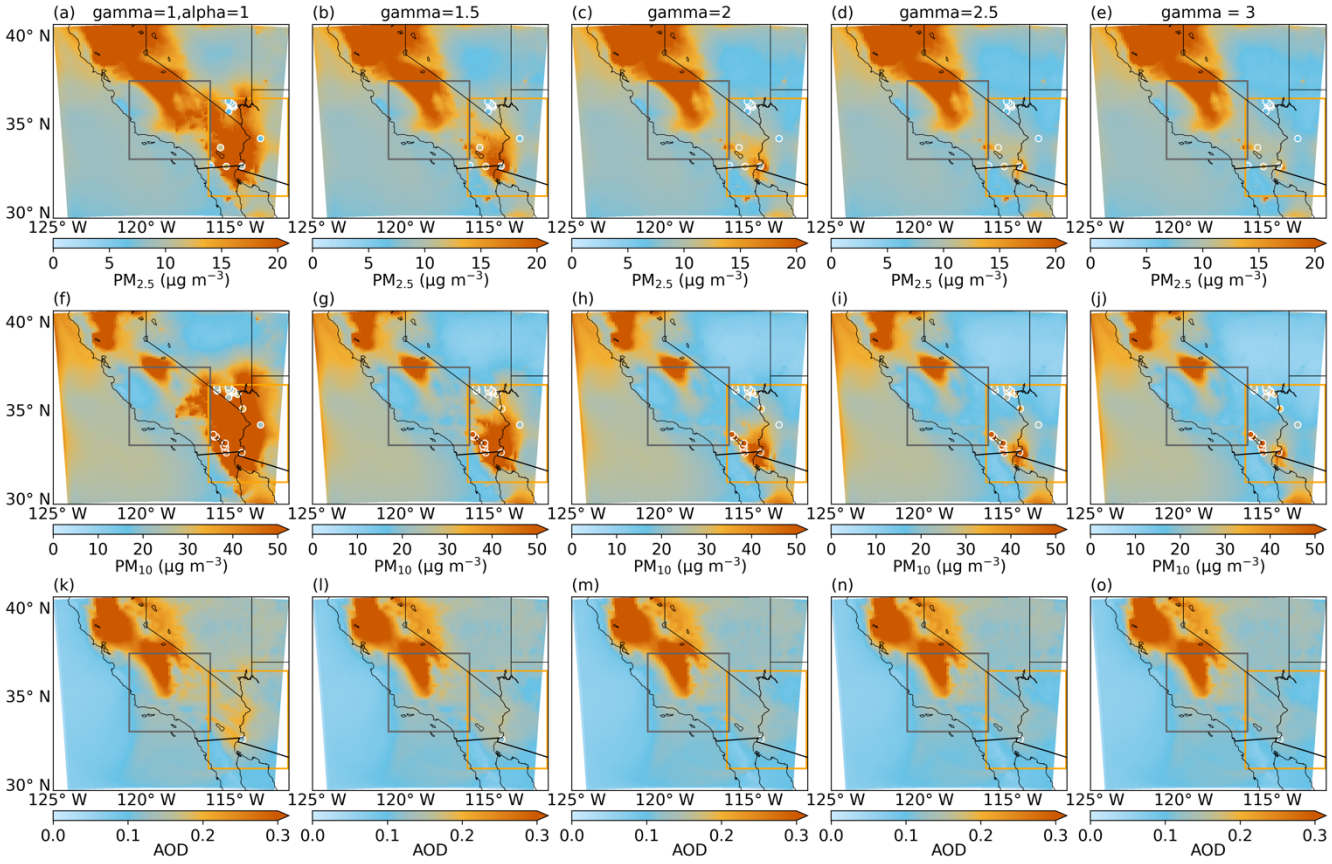

190 Figure S13. UI-WRF-Chem simulated monthly mean surface PM concentration and AOD overlaid with ground observations denoted as the solid circles over the outer domain (D1) of USA-LosAngeles in July 2018 from the group of sensitivity simulations that gamma value is set as 1, 1.5, 2, 2.5 and 3 while alpha value stays as 1. (a)–(e) are for surface $PM_{2.5}$ concentration, (f)–(j) are for surface PM_{10} concentration, and (k)–(o) are for AOD. The gray box represents the inner domain (D2), and the orange box represents the dust-prone region where we focus on dust emission tuning.

195

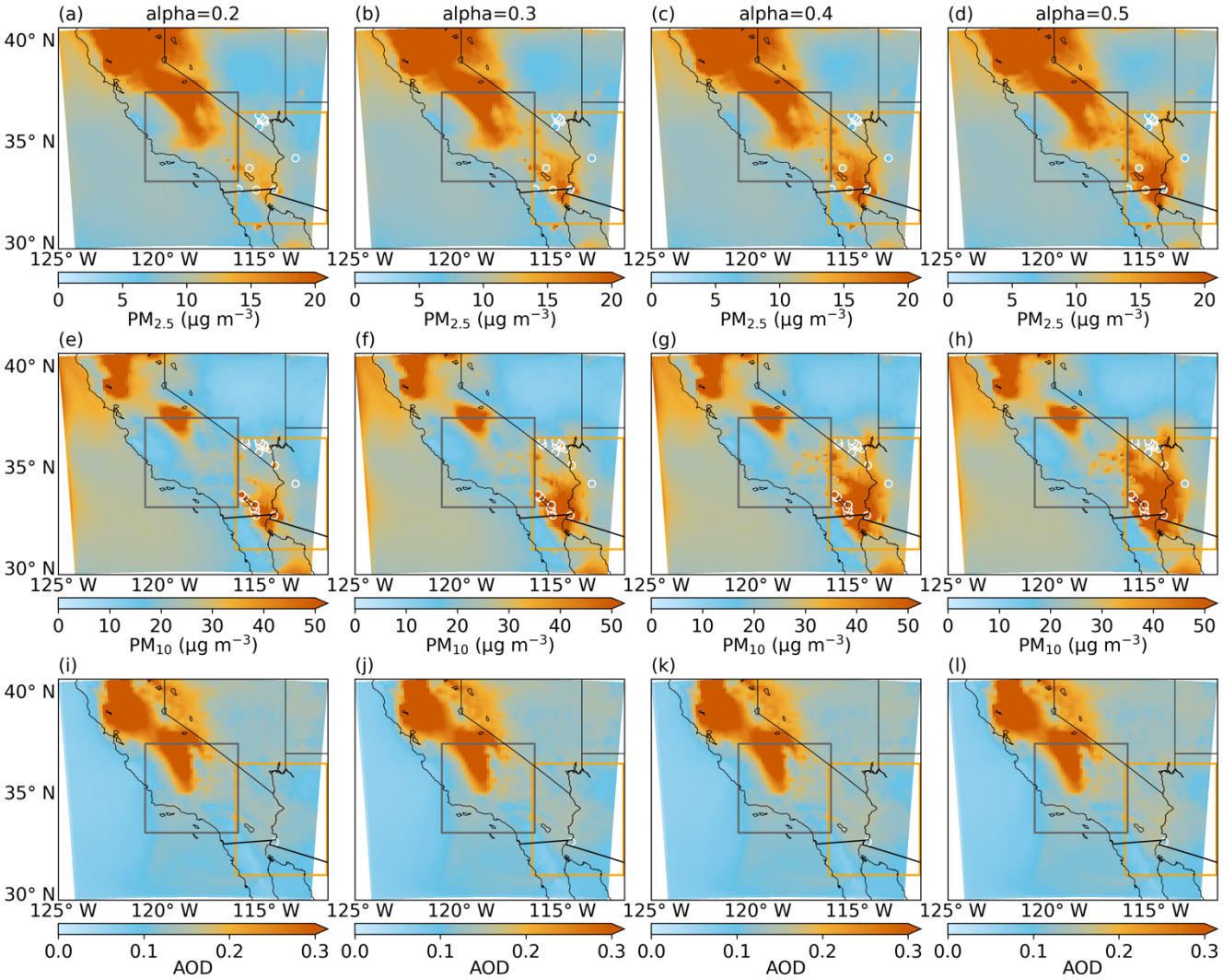

Figure S14. UI-WRF-Chem simulated monthly mean surface PM concentration and AOD overlaid with ground observations denoted as the solid circles over the outer domain (D1) of USA-LosAngeles in July 2018 from the group of sensitivity simulations that alpha value is set as 0.2, 0.3, 0.4 and 0.5 while gamma value stays as 1. (a)–(d) are for surface $PM_{2.5}$ concentration, (e)–(h) are for surface PM_{10} concentration, and (i)–(l) are for AOD. The gray box represents the inner domain (D2), and the orange box represents the dust-prone region where we focus on dust emission tuning.

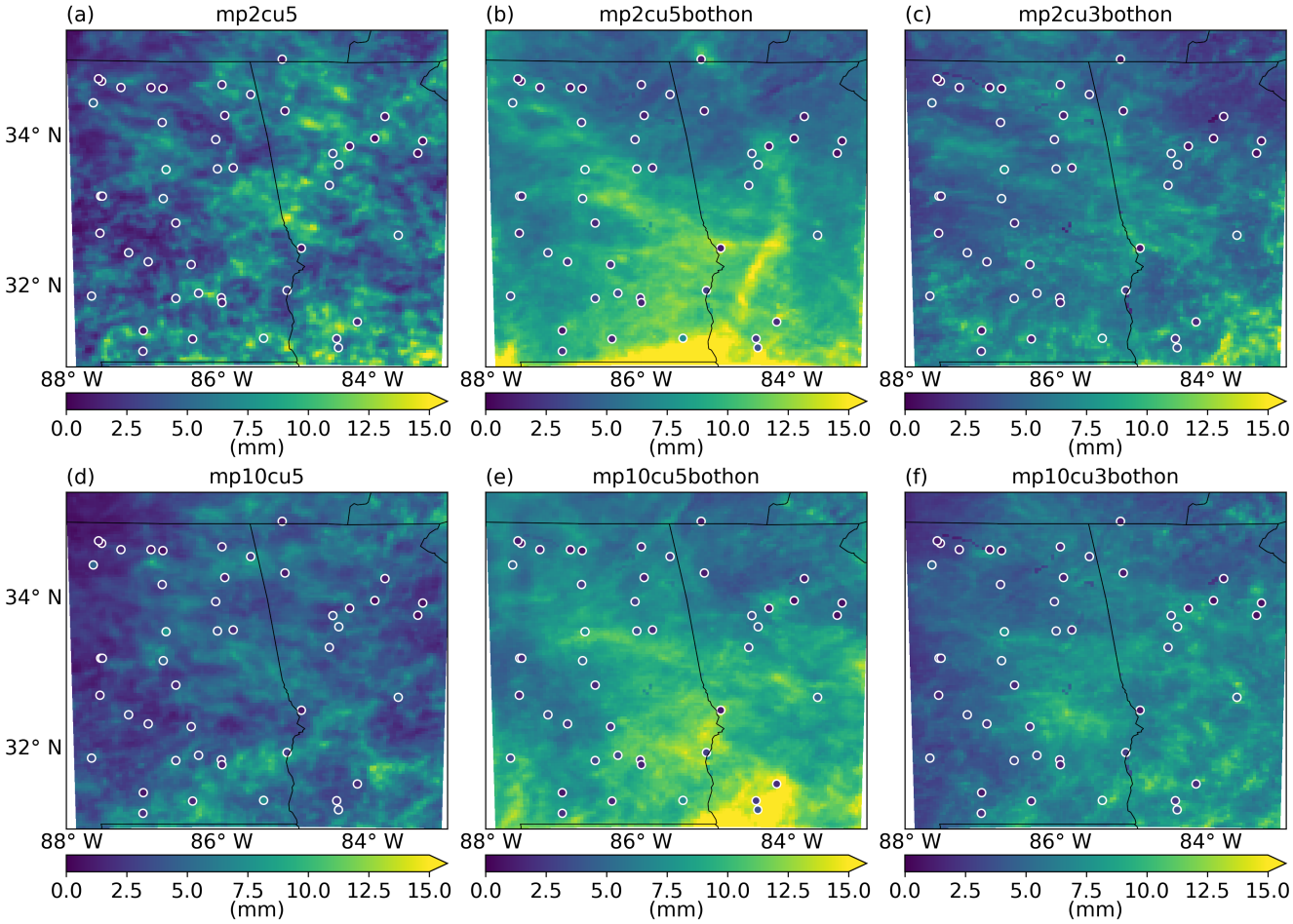

Figure S15. UI-WRF-Chem simulated monthly mean daily precipitation overlaid with ground observations denoted as the solid circles over the inner domain (D2) of USA-Atlanta for June 2022. (a)–(f) are the UI-WRF-Chem sensitivity simulations with different setups of microphysics and cumulus schemes. (a)–(c) all have the Lin microphysics scheme on for domain 1. (a) has the Lin microphysics scheme on for domain 2 and no cumulus scheme is used for domain 2. (b) is the same as (a) except that the G3D cumulus scheme is turned on for domain 2. (c) is same as (b) except that the GF cumulus scheme is used for domain 2. (d)–(f) are the same as (a)–(c) except that the Morrison microphysics scheme is used for both domain 1 and domain 2.

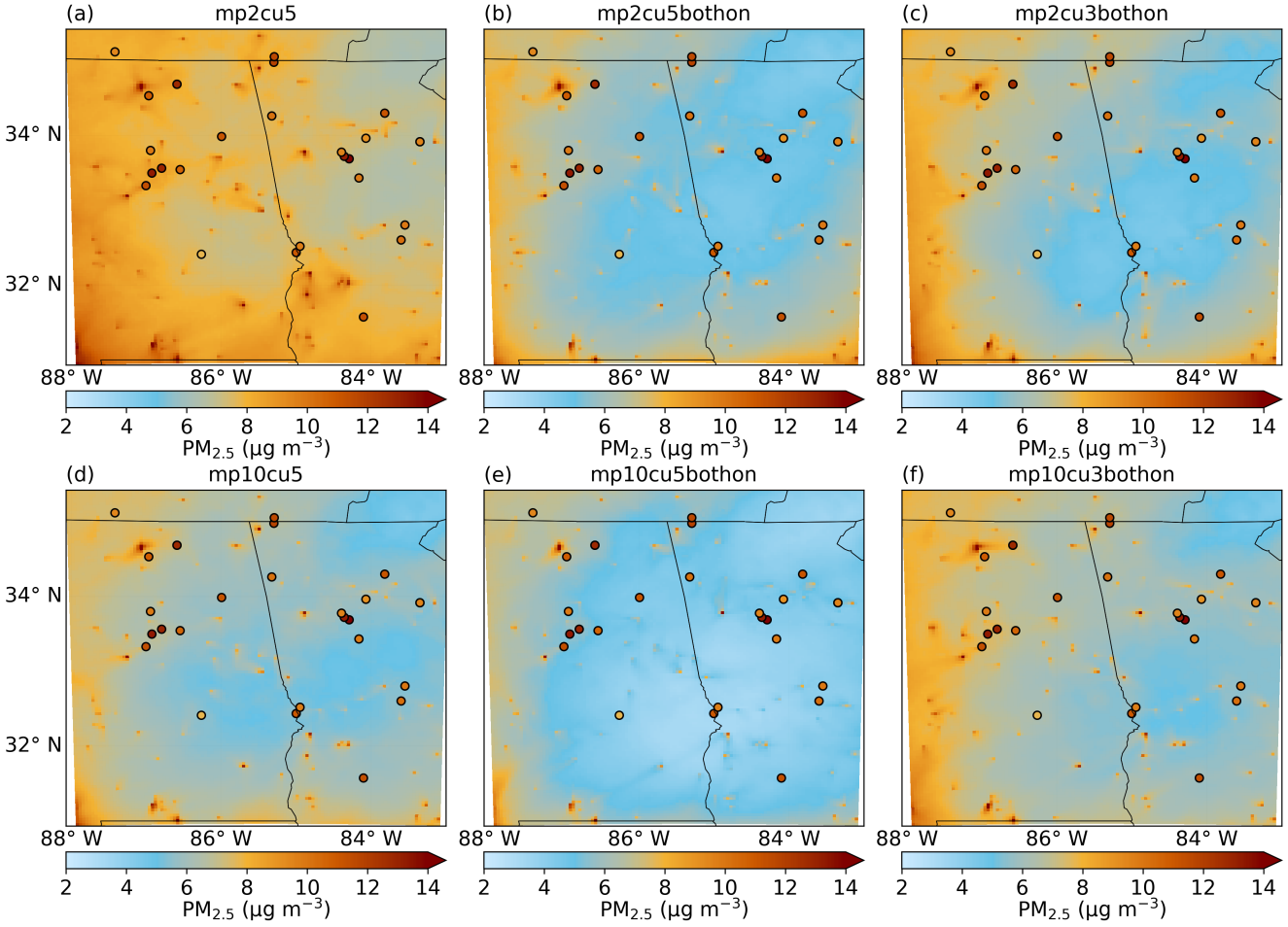

Figure S16. Same as Fig S15 but for surface $PM_{2.5}$ concentration.

215

References

Chen, D., Xie, X., Zhou, Y., Lang, J., Xu, T., Yang, N., Zhao, Y., and Liu, X.: Performance evaluation of the WRF-Chem model with different physical parameterization schemes during an extremely high PM2. 5 pollution episode in Beijing, Aerosol and Air Quality Research, 17, 262-277, 2017.

Dubovik, O. and King, M. D.: A flexible inversion algorithm for retrieval of aerosol optical properties from Sun and sky radiance measurements, Journal of Geophysical Research: Atmospheres, 105, 20673-20696, https://doi.org/10.1029/2000JD900282, 2000.

Friedl, M. A., McIver, D. K., Hodges, J. C. F., Zhang, X. Y., Muchoney, D., Strahler, A. H., Woodcock, C. E., Gopal, S., Schneider, A., Cooper, A., Baccini, A., Gao, F., and Schaaf, C.: Global land cover mapping from MODIS: algorithms and early results, Remote Sensing of Environment, 83, 287-302, https://doi.org/10.1016/S0034-4257(02)00078-0, 2002.

Holben, B. N., Eck, T. F., Slutsker, I., Tanre, D., Buis, J., Setzer, A., Vermote, E., Reagan, J., Kaufman, Y., and Nakajima, T.: AERONET—A federated instrument network and data archive for aerosol characterization, Remote sensing of environment, 66, 1-16, 1998.

Hou, A. Y., Kakar, R. K., Neeck, S., Azarbarzin, A. A., Kummerow, C. D., Kojima, M., Oki, R., Nakamura, K., and Iguchi, T.: The Global Precipitation Measurement Mission, Bulletin of the American Meteorological Society, 95, 701-722, https://doi.org/10.1175/BAMS-D-13-00164.1, 2014.

Hsu, N., Lee, J., Sayer, A., Kim, W., Bettenhausen, C., and Tsay, S. C.: VIIRS Deep Blue aerosol products over land: Extending the EOS long-term aerosol data records, Journal of Geophysical Research: Atmospheres, 124, 4026-4053, 2019.

Winker, D. M., Vaughan, M. A., Omar, A., Hu, Y., Powell, K. A., Liu, Z., Hunt, W. H., and Young, S. A.: Overview of the CALIPSO mission and CALIOP data processing algorithms, Journal of Atmospheric and Oceanic Technology, 26, 2310-2323, 2009.